**Tree Physiology** 27, 1505–1516


# Mechanical analysis of the strains generated by water tension in plant stems. Part I: stress transmission from the water to the cell walls

TANCRÈDE ALMÉRAS[1,2] and JOSEPH GRIL[3]

[1] *INRA-UMR Ecofog, Campus Agronomique, BP 316, 97379 Kourou Cedex, French Guiana, France*

[2] *Corresponding author (t_almeras@hotmail.com)*

[3] *LMGC, Université Montpellier 2, Montpellier, France*

Received November 24, 2006; accepted March 10, 2007; published online August 1, 2007

**Summary** Plant tissues shrink and swell in response to changes in water pressure. These strains can be easily measured, e.g., at the surface of tree stems, to obtain indirect information about plant water status and other physiological parameters. We developed a mechanical model to clarify how water pressure is transmitted to cell walls and causes shrinkage of plant tissues, particularly in the case of thick-walled cells such as wood fibers. Our analysis shows that the stress inside the fiber cell walls is lower than the water tension. The difference is accounted for by a stress transmission factor that depends on two main effects. The first effect is the dilution of the stress through the cell wall, because water acts at the lumen border and is transmitted to the outer border of the cell, which has a larger circumference. The second effect is the partial conversion of radial stress into tangential stress. Both effects are quantified as functions of parameters of the cell wall structure and its mechanical properties.

*Keywords: biomechanics, cell mechanics, diurnal strains, mechanical model, multilayer cylinder, stress transmission factor.*

## Introduction

Water inside terrestrial plants is generally in a state of tension, i.e., negative pressure (Tyree and Zimmerman 2002). The onset of this negative pressure is related to evaporation at the leaf surface. Evaporation induces a drop in leaf water potential, and thus a suction force that propagates down to the roots, facilitating soil water uptake. Water tension transports water from the soil to the leaves and undergoes large diurnal and seasonal variations in response to physiological regulation and environmental fluctuations. The propagation of this negative pressure is made possible because of the high tensile strength of water (Tyree and Zimmerman 2002), i.e., the bonding of water molecules to each other. Water is also closely bonded to plant cell walls, so that the water tension is, at least partly, transmitted to the solid medium in which it is contained. This is the basis of turgor pressure in living cells, where the osmotic pressure is balanced by the mechanical action of the cell wall on water. The transmission of pressure from a fluid through solid cell walls is the principle underlying the measurement of plant water potential with a pressure chamber (Scholander et al. 1964, Cochard et al. 2001).

The transmission of pressure from a fluid through solid cell walls also causes shrinkage and swelling of plant tissues in response to changes in water status. This phenomenon has long been recognized in trees, because diurnal variation in stem diameter (hereafter termed diurnal strain) in response to physiological activity is easily detected (Klepper et al. 1971, Ueda and Shibata 2001). Diurnal strain measurements are potentially a powerful tool for studying tree physiology, because they are nondestructive and can be monitored continuously with strain gages (Okuyama et al. 1995, Yoshida et al. 2000*a*) or linear transducers (Klepper et al. 1971, Daudet et al. 2005) to obtain spatial and temporal patterns of physiological activity (Sevanto et al. 2002). Diurnal strains have been considered, in terms of their effects on wood morphogenesis (Okuyama et al. 1995, Abe and Nakai 1999, Yoshida et al. 2000*b*, 2000*c*, Abe et al. 2001), relationships with phloem sugar transport (Sevanto et al. 2003, Daudet et al. 2005) and reduced wood conductivity (Ueda and Shibata 2002, Hölttä et al. 2002), as well as practical applications, such as correcting dendrometric data (Kozlowsky and Winget 1964, Downes et al. 1999, Deslauriers et al. 2003), and irrigation scheduling (Goldhammer and Fereres 2001, Remorini and Massai 2003).

The relationship between changes in stem water potential and strains measured at the surface of a tissue can be quantified empirically (So et al. 1979, Irvine and Grace 1997, Cochard et al. 2001, Alméras et al. 2006). However, because of the variability in plant materials and the time courses of their development, this relationship is not constant, making multiple, time-consuming calibrations necessary. It has been suggested that the resulting calibration factor is related to the elastic properties of the swelling tissues (So et al. 1979, Neher 1993, Irvine and Grace 1997); however, the relationship between water potential and strain at the stem surface is not straightforward, and no explicit formulation of the related mechanical problem has yet been provided. In this paper, we present a rig-

orous formulation and resolution of the mechanical problem of calculating the state of equilibrium of a structure subjected to internal stress and to external constraints at its borders. We formulated the mechanical problem in a general way, so that it can be applied to other biomechanical problems involving a cylindrical porous structure made of orthotropic material subjected to variation in pressure in its liquid phase. The simplified formula, derived from this model by taking into account the morphological and mechanical properties of plant stems, should allow independent estimation of the calibration factor linking strains and stem water potential.

## Mechanical behavior of a cylinder submitted to internal stress

### *Mechanical problems associated with the effect of water pressure in trees*

Our reference material is the woody stem of a dicotyledonous plant. A portion of the woody stem can be idealized as a cylinder, having a uniform structure in the longitudinal direction and radial symmetry. However, the structure is not uniform in the radial direction because it bears a succession of tissues of different ages, structures, functions and mechanical properties (pith, heartwood, sapwood, phloem and other extra-cambial tissues). Therefore, we modeled a stem portion as a multi-layered cylinder, assuming longitudinal and tangential homogeneity but accounting for radial heterogeneity.

A typical feature of plant materials is their anisotropy. They are organized along specific directions (longitudinal, radial and tangential). Their mechanical properties strongly depend on the direction considered. For example, wood is typically 10 to 20 times stiffer in the longitudinal direction than in the radial direction and 1.5 to 2 times stiffer in the radial direction than in the tangential direction. Therefore, woody stems must be considered orthotropic. In addition, couplings exist between the various directions, both at the material level (Poisson's ratio) and at the structural level (dependence between radial displacement and tangential strain inside a cylinder). These coupling effects may have important consequences for the distribution of stresses and strains.

Another characteristic of plant vascular tissues is porosity. A macroscopic volume of material essentially contains cell walls and lumens. Lumens are filled with sap and connected to each other. Because of tension forces, water adheres to the internal surfaces of the lumens so that any force applied to the liquid phase (water) is transmitted to the solid phase (cell walls). From a macroscopic standpoint, the plant tissue appears as a two-phase system subjected to internal forces. To account for internal forces, a specific formulation is required where some inelastic "induced" stress is considered in the macroscopic material.

To solve the complete problem, a two-level approach is necessary. At the stem level, one can predict the strains and residual stress in the structure caused by a known induced stress for given boundary conditions. Computation of the field of internally induced stress is a prerequisite. This internally induced stress is not exactly equal to the change in water pressure, because the solid phase (cell walls) must also be accounted for. The stress induced in the material at the macroscopic level can be computed by considering, at the cell level, the transmission of stress from the liquid to the solid phase.

Fortunately, the problem at the cell level is closely analogous to that at the stem level because most vascular elements can be regarded as cylindrical structures made of multiple layers of anisotropic material. Therefore, the mechanical equations at both the stem and cell levels can be solved with the same basic model. The model is first used at the cell level to compute the stress induced in the material, and then at the stem level to compute the resulting field of strains inside the whole structure. In this paper, the model formulation and resolution and its application at the cell level are presented. The formulations and results provide a rational basis for understanding cell mechanics and may stimulate efforts to model related problems in plant physiology, such as the collapse of cells under large tensions, and the mechanisms underlying water potential measurements made with pressure chambers (Scholander et al. 1964). Application of the model to diurnal strains at the stem level will be presented elsewhere (Alméras 2008). The mechanical problem is analogous to those developed at the fiber or stem level in wood mechanics for modeling wood drying or maturation strains (Barber 1968, Archer 1987, Yamamoto 1998, Yamamoto et al. 2001, Alméras et al. 2005). Many elements of the formulation proposed in this paper are derived from those given by Archer (1987).

A rigorous mathematical formulation of the model is provided to allow identification of the main assumptions on which it is based and derive general solutions. The model is then used to simulate the effects of various parameters based on data from the literature. When possible, simplified models are derived and validated from this general formulation to provide useful, tractable analytical tools.

### *Formulation of the mechanical problem*

The mechanical problem consists in computing the state of equilibrium of a structure subjected to internal stress and to external constraints at its borders. We first aim to solve the mechanical problem for a single homogeneous layer and then present solutions for a multilayer structure.

Under the action of internal and external stresses, any elementary volume of material tends to be displaced to a new equilibrium position. Spatial distribution of the displacements is described by the displacement field and the strain field derived from it. Because all displacements are not geometrically compatible, some residual stress appears. The objective of the mechanical problem is to compute these fields of displacement, strain and stress.

Let us consider a cylinder made of orthotropic material. The reference system associated with the cylindrical structure is noted $(R, T, L)$, where $R$ is the radial direction, $T$ the tangential direction and $L$ the longitudinal direction. Because no shear stress is induced, no shear stress or strain occurs so all expressions will be reduced to their normal components along direc-

tions $R$, $T$ and $L$. Because only small strains are involved, we also assume linear elastic behavior of the material.

*Displacements, strains, stresses and material properties*

At mechanical equilibrium, the displacement of the material at a given position is represented by the vector ($u_R$, $u_T$, $u_L$), the strain by ($\varepsilon_R$, $\varepsilon_T$, $\varepsilon_L$) and the residual stress by ($\sigma_R$, $\sigma_T$, $\sigma_L$) (symbols and their definitions are listed in Table A1). The stress initially induced in the material at a given position is noted ($\beta_R$, $\beta_T$, $\beta_L$). Elastic properties of the material quantify linear relationships between stress, strain and induced stress at a given position. They define the behavior law of the material as:

$$\begin{cases} \sigma_R = C_{RR}\varepsilon_R + C_{RT}\varepsilon_T + C_{LR}\varepsilon_L + \beta_R \\ \sigma_T = C_{RT}\varepsilon_R + C_{TT}\varepsilon_T + C_{TL}\varepsilon_L + \beta_T \\ \sigma_L = C_{LR}\varepsilon_R + C_{TL}\varepsilon_T + C_{LL}\varepsilon_L + \beta_L \end{cases} \quad (1)$$

where $C_{XY}$ are the stiffness terms characterizing the material properties. Diagonal terms $C_{XX}$ express the linear relationship between stress and strain along a given direction. Cross-terms $C_{XY}$ express the material coupling between directions $X$ and $Y$, i.e., the amount of stress generated in direction $Y$ when the material is strained in direction $X$. They are related to the usual engineering constants (moduli of elasticity and Poisson's ratios) by classical formulas (Bodig and Jaine 1982, Guitard 1987).

Strain, stress and stiffness terms are three-dimensional fields, i.e., they are defined at any position ($r$, $t$, $l$) inside the structure. However, because of cylindrical symmetries, they are assumed uniform along directions $T$ and $L$ so that they depend only on $r$. For a single homogeneous layer, we additionally assume that stiffness and induced stress are uniform along the $R$ direction, and are therefore defined as constant values.

*Field of displacement, strains and kinematic compatibility*

The basic parameter on which the resolution is based is the displacement vector ($u_R$, $u_T$, $u_L$). Fields of strain and stress will be derived from it. Because no shear stress is considered, it is apparent that no torsion occurs, so that the tangential displacement $u_T$ is null at any position inside the cylinder. We also assume that the longitudinal displacement $u_L$ is uniform in the $RT$ plane, meaning that a section remains planal during the deformation. This statement, referred to as the plane strain assumption, is generally verified inside a slender cylindrical structure except at its extremities, provided constitutive elements are mechanically connected in the transverse plane. For the same reason, the longitudinal strain $\varepsilon_L$ is uniform along $R$. Because of the cylindrical symmetries, the radial displacement $u_R$ does not depend on the tangential or longitudinal positions. The problem is then reduced to the determination of the constant longitudinal strain $\varepsilon_L$ and the radial displacement at any radial position, $u_R(r)$.

The radial strain derives from the radial displacement as:

$$\varepsilon_R(r) = \frac{du_R}{dr} \quad (2)$$

Inside a cylinder, radial and tangential strains are not independent of each other (see Appendix), but are linked by:

$$\varepsilon_T(r) = \frac{u_R}{r} \quad (3)$$

*Expression of static equilibrium*

The condition for static equilibrium inside a cylinder implies that (see Appendix):

$$\frac{d\sigma_R}{dr} + \frac{\sigma_R - \sigma_T}{r} = 0 \quad (4)$$

By inserting the behavior law (Equation 1) and replacing transverse deformations by their expressions given in Equations 2 and 3, the condition for static equilibrium (Equation 4) is reduced to:

$$r\frac{d^2u_R}{dr^2} + \frac{du_R}{dr} - \gamma^2\frac{u_R}{r} = K_\beta + K_L\varepsilon_L \quad (5)$$

where $\gamma$, $K_\beta$, and $K_L$ are constants defined in the Appendix. Equation 5 is a second-order differential equation, defining the field of radial displacement $u_R(r)$ at equilibrium. A general solution for this equation, assuming $\gamma \neq 1$ (Archer 1987) is:

$$u_R(r) = Ar^\gamma + Br^{-\gamma} + \frac{rK_\beta + \varepsilon_L K_L}{1-\gamma^2} \quad (6)$$

where $A$ and $B$ are integration constants. The values of $A$, $B$ and $\varepsilon_L$ are determined using the boundary conditions of the problem. This point will be clarified in the multi-layer formulation. The field of strain can be directly derived from the expression of $u_R(r)$ with Equations 2 and 3, and the field of stress can be derived with Equation 1.

## Mechanical behavior of a multilayer cylindrical structure

*Static equilibrium inside each layer*

Let us consider a cylindrical structure made of $n$ embedded layers, with external radii $r_1$, .., $r_n$. The inner radius of the innermost layer is noted $r_o$ (it is 0 if the cylinder is full). Each layer is assumed to have homogeneous material properties and is subjected to a homogeneous field of induced stress. Equation 6 gives the field of radial displacement for a given layer $i \in \{1...n\}$. Writing this equation for each layer results in a set of expressions containing $2n$ unknown integration constants ($A_i$ and $B_i$) and the unknown longitudinal strain $\varepsilon_L$. These $2n + 1$ unknown parameters are determined by interface and boundary conditions. The radial displacement and stress fields can be written, for $r \in [r_{i-1}, r_i]$:

$$u_R(r) = A_i\, a_i(r) + B_i\, b_i(r) + \varepsilon_L\, c_i(r) + d_i(r) \quad (7)$$

$$\sigma_R(r) = A_i\, e_i(r) + B_i\, f_i(r) + \varepsilon_L\, g_i(r) + h_i(r) \quad (8)$$

where $a_i$, $b_i$, $c_i$, $d_i$, $e_i$, $f_i$, $g_i$ and $h_i$ are known functions of $r$ defined in the Appendix.

*Conditions at the interfaces between layers*

At the interface between consecutive layers, the kinematic compatibility implies the continuity of radial displacement (meaning that the layers do not overlap and that no gap appears between layers), so that at $r_i$, for $i \in [1, n-1]$:

$$\begin{aligned} u_R(r_i) &= A_i\, a_i(r_i) + B_i\, b_i(r_i) + \varepsilon_L\, c_i(r_i) + d_i(r_i) \\ &= A_{i+1}\, a_{i+1}(r_i) + B_{i+1}\, b_{i+1}(r_i) + \varepsilon_L\, c_{i+1}(r_i) + d_{i+1}(r_i) \end{aligned} \quad (9)$$

Static equilibrium at the interface implies the continuity of radial stress, at $r_i$, for $i \in [1, n-1]$:

$$\begin{aligned} \sigma_R(r_i) &= A_i\, e_i(r_i) + B_i\, f_i(r_i) + \varepsilon_L\, g_i(r_i) + h_i(r_i) \\ &= A_{i+1}\, e_{i+1}(r_i) + B_{i+1}\, f_{i+1}(r_i) + \varepsilon_L\, g_{i+1}(r_i) + h_{i+1}(r_i) \end{aligned} \quad (10)$$

These relationships define $2n-2$ continuity conditions at the interfaces.

*Boundary conditions*

Radial boundary conditions of the whole structure are defined at the internal bound of the innermost layer ($r = r_0$) and at the external bound of the outermost layer ($r = r_n$). Depending on the particular problem considered, these conditions can be either imposed radial stresses $\sigma_o$ and $\sigma_n$ or imposed radial displacements $u_0$ and $u_n$. The "imposed stress" condition is used if the border is submitted to known external forces (e.g., the lumen water pressure) or if it is free of stress (the external border of a stem or the internal border of a hollow stem). If full kinematic restraint exists (as at the center of a full cylinder), the "imposed null displacement" condition is used.

The condition at the internal radial bound is:

$$u_R(r_0) = A_1\, a_1(r_0) + B_1\, b_1(r_0) + \varepsilon_L\, c_1(r_0) + d_1(r_0) = u_0 \quad (11)$$

or

$$\sigma_R(r_0) = A_1\, e_1(r_0) + B_1\, f_1(r_0) + \varepsilon_L\, g_1(r_0) + h_1(r_0) = \sigma_0 \quad (12)$$

The condition at the external radial bound is:

$$u_R(r_n) = A_n\, a_n(r_n) + B_n\, b_n(r_n) + \varepsilon_L\, c_n(r_n) + d_n(r_n) = u_n \quad (13)$$

or

$$\sigma_R(r_n) = A_n\, e_n(r_n) + B_n\, f_n(r_n) + \varepsilon_L\, g_n(r_n) + h_n(r_n) = \sigma_n \quad (14)$$

A last condition is given by the static equilibrium in the longitudinal direction. Again, two kinds of boundary conditions can be considered, either an imposed load or an imposed strain. In the case of an imposed strain, the value of $\varepsilon_L$ is directly given as input data. In the case of an imposed load, static equilibrium implies that the sum of all longitudinal stress over a section is equal to the variation of axial load $N$. We define $j_i$, $k_i$, $l_i$ and $m_i$, known functions of $r$ (see Appendix), so that static equilibrium in the longitudinal direction is given by:

$$\begin{aligned} &\sum_{i=1}^{n} \big(j_i(r_i) - j_i(r_{i-1})\big) A_i + \big(k_i(r_i) - k_i(r_{i-1})\big) B_i \\ &\quad + \big(l_i(r_i) - l_i(r_{i-1})\big) \varepsilon_L + \big(m_i(r_i) - m_i(r_{i-1})\big) = N \end{aligned} \quad (15)$$

*Complete resolution*

After choosing the relevant radial boundary conditions, Equations 9–15 define $2n+1$ interface and boundary conditions. They form a linear system with $2n+1$ equations and $2n+1$ unknown parameters ($\varepsilon_L$ and the integrations constants $A_i$ and $B_i$). These can be deduced by inversion of the linear system. All fields of stress, strain and displacement can be deduced from these quantities with Equations 1, 2, 3, 7 and 8. Input parameters of the model are the three boundary conditions ($N$, $u_o$ or $\sigma_o$, $u_n$ or $\sigma_n$) and, for each layer, its radius, stiffness terms and induced stresses.

## Numerical study of the stress induced in a standard wood fiber

*Application of the model at the cell level*

The cell wall is multilayered. The relationship between the water pressure in a cell lumen and stress induced in a material comprising many cells can be computed with the multi-layer cylinder model and appropriate sets of input parameters and boundary conditions. The equilibrium of the lumen–cell wall interface implies that radial stress at the internal radial bound of the cell is equal to the imposed water pressure $P$. The sign of the pressure is usually expressed using the conventions of hydraulics (where a compression is a positive pressure), so that, to be consistent with the conventions of mechanics of solids (where a tension is a positive stress), the boundary condition at the cell–lumen interface is given by Equation 12 with $\sigma_0 = -P$.

Next, we quantify the induced stress at the material level. For this, we assume that the cell is an elementary representative volume of the plant tissue and use the principle of homogenization. Macroscopic induced stress is an inelastic stress, i.e., a stress that appears without macroscopic strain in the material. It is equivalent to the stress generated at the external boundary of the cell, assuming it is completely restrained in displacement. Therefore, boundary conditions used for this problem are an imposed null displacement at the external radial bound (Equation 13 with $u_n = 0$) and an imposed null longitudinal strain ($\varepsilon_L = 0$).

*Parameter set for a standard wood fiber*

For a material made of identical cylindrical cells, the density $d$ is related to the cell wall thickness through the ratio of lumen radius to cell radius $\rho$ and the density of the cell wall material

$d_o$. Neglecting the gaps at the junctions of round cells, this relationship is:

$$\rho = \sqrt{1 - \frac{d}{d_0}} \tag{16}$$

In wood, most of the volume generally comprises fibers (or tracheids in gymnosperms). Our reference set of parameters describes the typical fiber of a hardwood as having a basic density $d = 650$ kg m$^{-3}$. Because the dry density of the wall material of wood fibers is close to $d_0 = 1500$ kg m$^{-3}$, the equivalent radius ratio is $\rho = 0.75$. The cell wall of a typical wood fiber is made of four layers (Figure 1). The outermost layer is made of the middle lamella and the primary wall and is referred to as the MP layer. Internal secondary layers are named, from outside to inside, $S_1$, $S_2$ and $S_3$. Each layer comprises a composite material with stiff cellulose microfibrils embedded in a matrix of lignin and hemicellulose. Cellulose microfibrils have a specific orientation relative to the cell axis, referred to as the microfibril angle (MFA). The microfibril content and angle of each layer used in this simulation are indicated in Table 1. Stiffness of the water-saturated cell wall material can be computed from these parameters with a cell-wall micro-mechanical model (Alméras et al. 2005). This model incorporates the shear restraint effect resulting from the juxtaposition of cells with anti-symmetric structure. The computed values used in the simulations are indicated in Table 1.

*Fields of transverse stress and strain inside the wall*

Fields of radial and tangential stress and strain inside the fiber wall (Figure 2) were computed in response to an arbitrary water tension of 1 MPa ($P = -1$ MPa). Because the formulation is linear, the magnitude of the computed fields of strain and stress is proportional to the value of the imposed tension. These results correspond to the virtual situation where the cell's outer border would be prevented from straining, because the aim in this section is to compute the macroscopically induced stress. From Figure 2, it is apparent that the radial stress and tangential strain are continuous functions of the radius, whereas tangential stress and radial strain exhibit discontinuities between layers. The radial stress at the lumen interface is equal to that of the water and decreases in a nonlinear fashion toward the middle lamella (Figure 3). The tangential stress is negative inside the inner $S_3$ layer and positive inside other layers. Its magnitude is lower inside the $S_1$ layer than inside other outer layers (Figure 2).

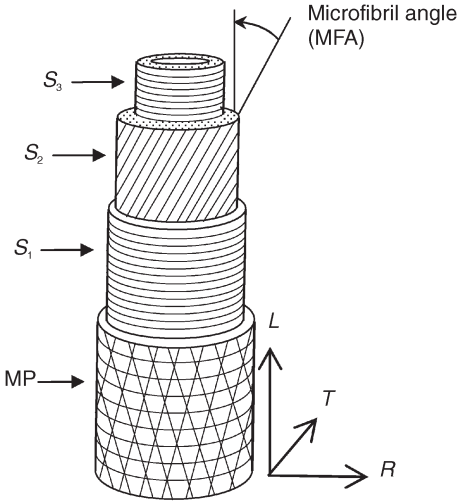


Figure 1. Schematic representation of a multilayer cylindrical wood fiber. Successive layers are the middle lamella and primary wall (MP), and three secondary layers ($S_1$, $S_2$, $S_3$) with different microfibril angle (MFA). The reference associated with the fiber is $R$ = radial, $T$ = tangential and $L$ = longitudinal direction.

Because the order of magnitude of water tension occurring in plant stems is at most only several MPa, it is apparent that the generated strains are small, which explains why a linear formulation is sufficient for this problem. Tangential strain is negative at the lumen interface (i.e., the lumen is smaller than before the onset of tension) and increases up to 0 toward the middle lamella.

The value of radial stress at the external border is equal to 75.5% of the water tension. This ratio is a parameter of interest because it allows conversion between the water tension and the stress induced in the material. Hereafter, we refer to it as the "stress transmission factor":

$$k = -\frac{\sigma_n}{P} \tag{17}$$

*Sensitivity of the stress transmission factor to fiber wall structure*

Figure 3 shows that the stress transmission factor depends on

Table 1. Parameters defining the structure of the reference fiber and the stiffness of its layers. Abbreviations: MP = middle lamella + primary wall; $S_1$, $S_2$, $S_3$ = secondary layers; $C_{RR}$ = radial stiffness; $C_{TT}$ = tangential stiffness; $C_{LL}$ = longitudinal stiffness; and $C_{RT}$, $C_{TL}$, $C_{LR}$ = coupling terms.

| | Thickness (% wall) | Microfibrils | | Stiffness terms (GPa) | | | | | |
|---|---|---|---|---|---|---|---|---|---|
| | | Content (%) | Angle (°) | $C_{RR}$ | $C_{TT}$ | $C_{LL}$ | $C_{TL}$ | $C_{LR}$ | $C_{RT}$ |
| MP | 10 | 10 | uniform | 3.5 | 8.1 | 8.1 | 2.7 | 1.3 | 1.3 |
| $S_1$ | 10 | 20 | 70 | 4.4 | 22.8 | 5.2 | 3.9 | 1.5 | 1.2 |
| $S_2$ | 70 | 35 | 15 | 5.6 | 5.8 | 42.9 | 4.0 | 1.2 | 1.9 |
| $S_3$ | 10 | 20 | 80 | 4.4 | 26.9 | 4.4 | 2.2 | 1.6 | 1.2 |

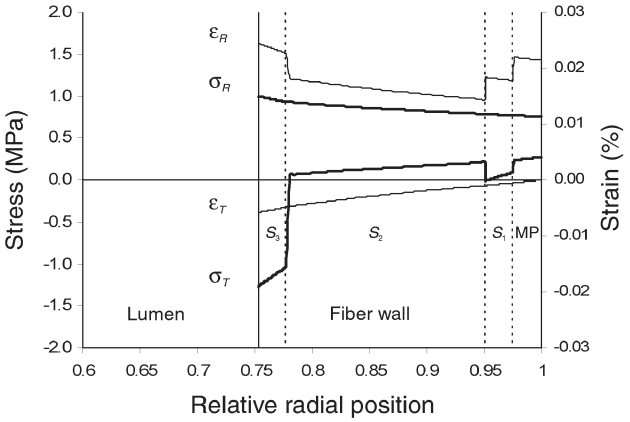


Figure 2. Fields of radial stress ($\sigma_R$), tangential stress ($\sigma_T$), radial strain ($\varepsilon_R$) and tangential strain ($\varepsilon_T$) inside the fiber wall, induced by a water tension of 1 MPa in the lumen, assuming the outer border of the cell is restrained. The radial position is standardized by the fiber radius. Abbreviations: MP = middle lamella + primary wall; and $S_1$, $S_2$, $S_3$ = secondary layers.

fiber wall thickness, because radial stress always decreases inside the wall. Wall thickness is related to density through Equation 16. The effect of basic density on $k$ is shown in Figure 4. The stress transmission factor tends to 1 when the density tends to 0, decreases nonlinearly with basic density and tends to 0 when the density tends to $d_o$ (i.e., when the lumen is reduced to a null radius).

The microfibril angle (MFA) of the $S_2$ layer varies among wood cell types and controls the tangential stiffness of the cell wall. Its effect was tested for a fixed basic density of 650 kg $m^{-3}$. As illustrated by Figure 5, $k$ tends to decrease slowly with increasing MFA and consequent increasing tangential stiffness.

Fields of tangential stress presented in Figure 2 show that the $S_3$ layer is strongly compressed. Also, the radial stress decreases more steeply inside the $S_3$ than inside other layers (Figure 3). Because this layer is adjacent to the lumen and has the highest MFA and consequently the highest tangential stiffness, it was suspected to be a sensitive parameter. The effect of its thickness on $k$ was tested for a standard density and MFA. As shown in Figure 6, the sensitivity of this parameter is low. Only a slight decrease in $k$ was observed with increasing thickness of the $S_3$ layer.

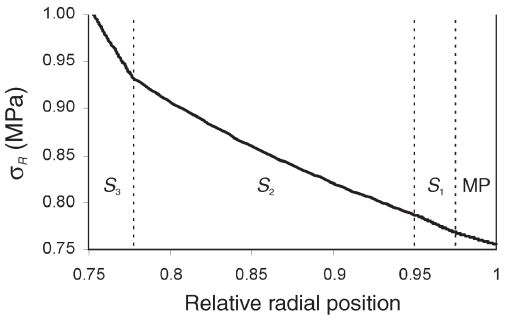


Figure 3. Enlargement of Figure 2 showing the field of radial stress ($\sigma_R$) inside the fiber wall, induced by a water tension of 1 MPa in the lumen, assuming the outer border of the cell is restrained. The radial position is standardized by the fiber radius. Abbreviations: MP = middle lamella + primary wall; and $S_1$, $S_2$, $S_3$ = secondary layers.

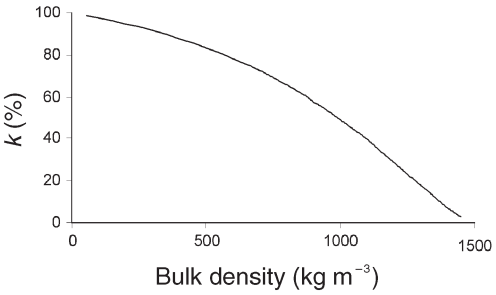


Figure 4. Variations in stress transmission factor ($k$) as a function of bulk density.

To summarize, $k$ in wood fibers is always less than 1, and it is decreased by a high density (i.e., large wall thickness) and a high MFA (i.e., high tangential/radial stiffness ratio). A straightforward quantification of these effects with a simplified analytic model is described in the next section.

## Simplified analytic model

### *Explicit model for a single layer*

The simplified analytic model is based on the representation of the cell wall as a single layer. The external radial stress $\sigma_1$, due to a tension $P$ at the lumen interface, can be made explicit by using Equations 12 and 13 for boundary conditions and solving Equation 8:

$$\sigma_1 = \frac{2\rho\gamma C_{RR} P}{\rho^{\gamma}\left(C_{RT} + \gamma C_{RR}\right) - \rho^{-\gamma}\left(C_{RT} - \gamma C_{RR}\right)} \tag{18}$$

If we neglect Poisson's ratio of the material (i.e., assuming $C_{RT}$ = 0), the stress transmission factor can be simplified as (combining Equations 1 and 18):

$$k = \frac{2\rho}{\rho^{\gamma} + \rho^{-\gamma}} \tag{19}$$

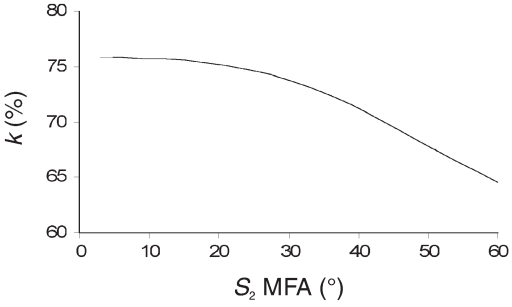


Figure 5. Variations in stress transmission factor ($k$) as a function of the microfibril angle (MFA) of the $S_2$ layer.

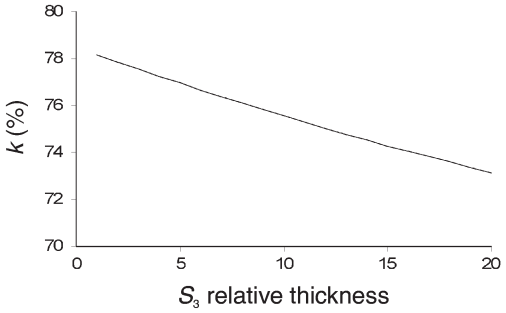


Figure 6. Variations in stress transmission factor ($k$) as a function of the relative thickness of the $S_3$ layer.

where ρ denotes the effect of cell wall thickness and γ denotes the effect of cell wall anisotropy.

*Effects of cell wall thickness and anisotropy on the radial stress transmission factor*

Figure 7 illustrates the effects of cell wall thickness and anisotropy on the radial stress transmission factor. It is apparent that, when the radial stiffness is larger than the tangential stiffness ($C_{RR}/C_{TT} > 1$), $k$ tends to a maximal value. However, if the tangential stiffness is larger than the radial stiffness (as it is usually the case for cell walls), $k$ is reduced, and this reduction is larger if the cell wall is thicker. For the standard hardwood fiber, the $C_{RR}/C_{TT}$ ratio of the wall ranges between 0.2 and 0.5, depending on the MFA, so that the reduction in stress transmission is negligible if the wall is thin, but becomes more substantial for a dense wood (Figure 7).

These effects can be interpreted by considering that radial stress is transmitted through radial connections between solid particles. If stiff tangential reinforcements are present, radial stress is partly converted into tangential stress, and is therefore not fully transmitted in the radial direction. This can be easily visualized when considering the two limiting cases illustrated by Figures 8A and 8B. These figures illustrate a virtual cell wall made only of tangential or radial reinforcements, with voids between them. In the case of the tangential reinforcements, no radial transmission of the lumen stress is possible, because reinforcements are mechanically isolated from each other in the radial direction. In the case of the radial reinforcements, each reinforcement transmits all the stress from the internal to the external border of the wall.

Moreover, if each radial reinforcement transmits all the radial stress from the internal to the external border, then the mean stress at the external border is lower than on the internal border, because it acts on a larger circumference. The radial stress transmission factor is then the ratio of lumen circumference to cell circumference, which is equal to ρ. This geometric consideration is consistent with the results of Equation 19 for the case where $\gamma = 0$.

The accuracy of this simplified analytic model can be appreciated in Figure 9 by comparison with the effect of density computed by the multi-layer model. The small discrepancy between the models results from the effect of the tangential stiffness previously mentioned, and from other complex mechanical effects caused by material couplings (cross stiffness terms) and 3D effects, which are neglected in the geometric model.

*Anisotropy of stress transmission*

We have considered a stress transmission factor based on radial stress. The computation of longitudinal stress is straightforward, because the water column and the cell wall act in parallel, so that their stresses can be added. The longitudinal stress inside the lumen is $P$. If ρ denotes the relative radius of the lumen, its relative area is $\rho^2$, and a good approximation of the mean stress in the longitudinal direction is given by:

$$\sigma_L = \rho^2 P \tag{20}$$

The longitudinal stress transmission factor is then:

$$k_L = \rho^2 \tag{21}$$

Comparison with Equation 19 shows that $k$ is not equal in the longitudinal direction or in the transverse plane, and is therefore not isotropic. Because we assumed cylindrical symmetry at the cell level, it was implicitly computed as transversely isotropic. However, the real field may also be macroscopically anisotropic in the transverse plane, because cell elements are not always cylindrical. Their real shape is generally polygonal

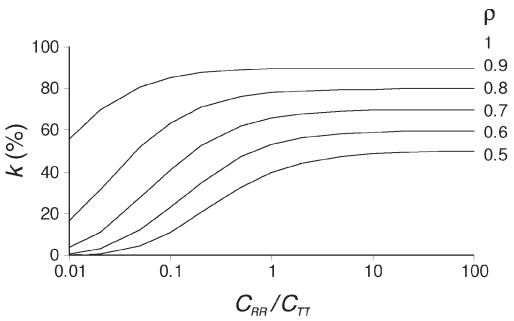


Figure 7. Variations of the stress transmission factor ($k$) as a function of the anisotropy ratio $C_{RR}/C_{TT}$ for various values of the radius ratio ρ.

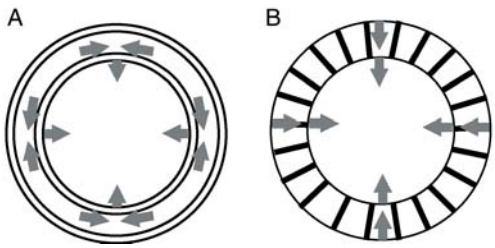


Figure 8. Simple models of fiber walls. (A) Wall made mainly of tangential reinforcements. Radial stress at the lumen interface is converted to tangential stress and is not efficiently transmitted through the fiber wall. (B) Wall made mainly of radial reinforcements. Radial stress at the lumen interface is fully transmitted through the fiber wall.

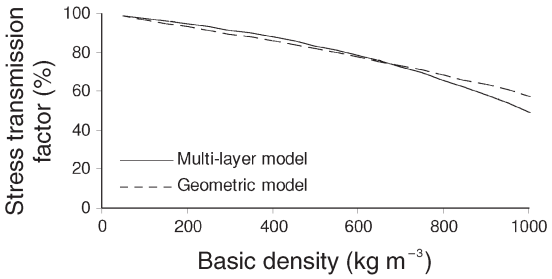


Figure 9. Comparison of the relationship between stress transmission factor and basic wood density for the simple geometric and multilayer model.

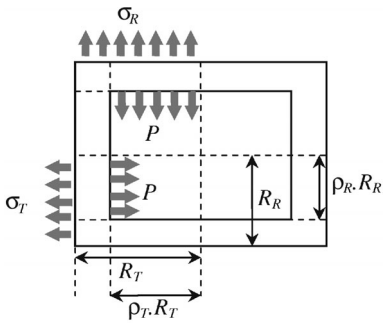


Figure 10. Model of an anisotropic rectangular cell. Neglecting the effect of cell corners, the external stress in each direction ($\sigma_R$, $\sigma_T$) caused by variation in pressure ($P$) inside the lumen can be roughly evaluated by a parallel model. Abbreviations: $R_R$ = half radial dimension; $R_T$ = half tangential dimension; $\rho_R$ = relative thickness of a radial wall; and $\rho_T$ = relative thickness of a tangential wall.

with rounded corners. The thickness or stiffness of the wall oriented in the macroscopic tangential direction may differ from that of the radial walls, as may the transmission factor.

The effect of cell geometry on the transmission factor can be evaluated with a simple rectangular model. Neglecting the effect of the cell corners, the external stress can be approximated by considering a parallel association between water and cell walls (Figure 10). Anisotropic transverse stress transmission factors are then:

$$k_R = \rho_T \tag{22}$$

$$k_T = \rho_R \tag{23}$$

where $\rho_R$ and $\rho_T$ are the respective ratios of radial and tangential lumen dimensions to fiber dimension. These results are consistent with the geometric effect for a circular cell, i.e., Equation 19 in the case where $\gamma = 0$.

## Discussion

### *Multilayer cylinder model*

Several models for computing the stress in a cell wall caused by lumen water tension have been developed in the context of wood technology to study the onset of collapse in drying wood. Innes (1995) developed a multilayer cylinder model that has many similar features to our model. The resolution of the problem was performed numerically by considering a series of thin cylindrical elements. This numerical resolution allowed the model to take into account the nonlinear behavior of the wood substance under large stress leading to failure (Innes 1995). A complementary approach was provided by Hunter (2001), who made the simplifying assumption that the wood substance was transversely isotropic, but accounted for the non-circular shape of the cell section. This option may bring interesting information about the effect of a departure from cylindrical symmetry; however, the assumption of an isotropic wall material is not suitable for the problem we studied because, as we demonstrated, wall anisotropy was an important parameter determining stress transmission across the cell wall.

### *Effects of tissue anisotropy and osmotic pressure*

Our mechanical model was illustrated by application to a fiber cell of a standard hardwood, but it can also be used to model the effect of water pressure on any type of cell, provided its shape can be approximated by a cylinder. We realize that a cylindrical element is an elementary representation of the volume of the material, and implicitly neglects the effect of the cell corners. An anisotropic description of the cell shape was briefly taken into account. In addition, the distribution of cell types in wood material is strongly anisotropic. For example, rays may be arranged as radial bands, and vessels as tangential bands. The difference in the stress transmission ratio of these elements results in an additional stress anisotropy at the wood level. This source of anisotropy may be quantified by simple mechanical models accounting for a series/parallel association of the tissues (Guitard and Gachet 2004). However, we consider that these are second-order effects and that transverse isotropy of macroscopic induced stress is a sufficient approximation. The main source of anisotropy of the actual strains in the plant material was caused not by anisotropy of the induced stress, which is low, but by the anisotropy of stiffness of the material. Stiffness anisotropy is large and cannot be neglected when computing the strains inside the material at a macroscopic level, but it does not need to be accounted for when computing the induced stress. This is the reason we chose to compute the stress induced inside a virtually restrained cell, instead of directly computing the strain induced inside a virtually isolated cell: these options are mathematically equivalent, but our approach allowed clear separation of the parameters involved at the microscopic and macroscopic levels.

When modeling living cells or phloem, the effect of osmotic pressure cannot be neglected because its magnitude is large and undergoes temporal and spatial variations (Sevanto et al. 2003). The effect of osmotic pressure is that, once the diffusion equilibrium is achieved, the hydrostatic pressure in the cell differs from that of the water outside the cell. If $P$ is the change in pressure inside the xylem water and $\pi$ the change in osmotic potential inside the living cells, then the change in hy-

drostatic pressure inside the cell is $P + \pi$ (Tyree and Zimmerman 2002). This kind of cell can be treated in the same way as the fiber cell, provided the cell membrane is semi-permeable and diffusion equilibrium has been reached.

*Stress transmission between the liquid and the solid phase*

The behavior of a cell wall undergoing a change in lumen water pressure was simulated with a multilayer cylinder model of orthotropic material. Our main goal was to compute $k$, to simulate the strains occurring at the plant stem level. The stress transmission factor depends mainly on two effects: a geometric effect and an effect of cell wall anisotropy. The geometric effect depends on cell wall thickness and then on tissue density. The geometric effect "dilutes" the radial stress at a rate equal to the ratio of lumen circumference to cell circumference. The effect of cell wall anisotropy reduces the radial stress transmission as a result of the conversion of radial stress into tangential stress. It can be non-negligible if the radial stiffness of the cell wall is much lower than its tangential stiffness (for example in the case of large microfibril angle) and the cell wall is thick.

A simple model was proposed to quantify these effects and compute $k$. At the macroscopic level, $k$ can be viewed as a mechanical property of a set of fibers, linking the pressure of lumen water to the stress induced in the material. This property depends on the same micro-structural parameter as the transverse stiffness of the material (namely the density and MFA), but not in the same way, so that it is a distinct property. In a standard wood fiber, the transverse $k$ was determined to be 0.75. Realistic values of this parameter for wood range from 0.5 for a dense wood with large microfibril angle to 0.9 for wood with low density.

*Heterogeneity of macroscopic stress and strain*

The model allows computation of the field of macroscopic stress induced in the whole stem, provided that the field of hydrostatic pressure (including the effect of osmotic potential) is known, as well as the properties of cell elements of each tissue. In a living tree, variations in hydrostatic and osmotic pressures are both heterogeneously distributed (Panterne et al. 1998, Sevanto et al. 2003). The heterogeneity of the field of induced stress depends on these heterogeneities and also on the heterogeneity of $k$. The resulting field of strain in the stem depends on this field of induced stress and on the stiffness of the tissues at the macroscopic level. In previous models of the relationship between diurnal strains and water pressure, it was assumed that water pressure and strains were directly related by the mechanical properties of the material at the macroscopic level (Neher 1993, Irvine and Grace 1997, Offenthaler et al. 2001, Perämäki et al. 2001, Hölttä et al. 2002); however, this approach neglects the effect of stress transmission through the cell wall (i.e., it was implicitly assumed that $k$ is uniformly equal to 1). We have now shown that the stress induced in the material is significantly lower (by 10 to 50%) than the water pressure, so that the material appears stiffer than if it were submitted to external forces.

In conclusion, our mechanical model is the first specifically developed for modeling diurnal strains in living trees. Therefore, the boundary conditions we used differ from those used by Innes (1995) and Hunter (2001) for a piece of drying wood. Also, because diurnal strains are small, elasticity is a sufficient descriptor of wood behavior, allowing us to use a simpler mathematical formulation than in the above-mentioned models. We provided an explicit analytic solution, adapted from the work of Archer (1987), that allowed implementation of efficient calculations and consideration of the role of each parameter. A comprehensive explanation of the phenomena involved at the cell level was provided, and simplified models were derived and validated.

**Acknowledgments**

This study was supported by grand-in-aid for scientific research No. 15.03742 from the Japanese Society for the Promotion of Science (JSPS). TA received a post-doctoral fellowship from the JSPS.

**References**

Abe, H. and T. Nakai. 1999. Effect of the water status within a tree on tracheid morphogenesis in *Cryptomeria japonica* D. Don. Trees 14:124–129.

Abe, H., T. Nakai, Y. Utsumi and A. Kagawa. 2001. Temporal water deficit and wood formation in *Cryptomeria japonica*. Tree Physiol. 23:859–863.

Alméras, T. 2008. Mechanical analysis of the strains generated by water tension in plant stems. Part II: strains in wood and bark and apparent compliance. Tree Physiol. In press.

Alméras, T., J. Gril and H. Yamamoto. 2005. Modeling anisotropic maturation strains in wood in relation to fiber boundary conditions, microstructure and maturation kinetics. Holzforschung 59: 347–353.

Alméras, T., M. Yoshida and T. Okuyama. 2006. Strains inside xylem and inner bark of a stem submitted to a change in hydrostatic pressure. Trees 20:460–467.

Archer, R.R. 1987. On the origin of growth stresses in trees. Part 1: micromechanics of the developing cambial cell wall. Wood Sci. Tech. 21:139–154.

Barber, N.F. 1968. A theoretical model of shrinking wood. Holzforschung 22:97–103.

Bodig, J. and B.A. Jaine. 1982. Mechanics of wood and wood composites. Van Nostrand Reinhold Company, New York, 712 p.

Cochard, H., S. Forestier and T. Améglio. 2001. A new validation of the Scholander pressure chamber technique based on stem diameter variations. J. Exp. Bot. 52:1361–1365.

Daudet, F.-A., T. Améglio, H. Cochard, O. Archilla and A. Lacointe. 2005. Experimental analysis of the role of water and carbon in tree stem diameter variations. J. Exp. Bot. 56:135–144.

Deslauriers, A., H. Morin, C. Urbinati and M. Carrer. 2003. Daily weather response of balsam fir (*Abies balsamea* (L.) Mill.) stem radius increment from dendrometer analysis in the boreal forests of Québec (Canada). Trees 17:477–484.

Downes, G., C. Beadle and D. Worledge. 1999. Daily stem growth patterns in irrigated *Eucalyptus globulus* and *E. nitens* in relation to climate. Trees 14:102–111.

Goldhammer, D.A. and E. Fereres. 2001. Irrigation scheduling protocols using continuously recorded trunk diameter measurements. Irrig. Sci. 20:115–125.

Guitard, D. 1987. Mécanique du matériau bois et composites. Cepadues Editions, Toulouse, France, 238 p.

Guitard, D. and C. Gachet. 2004. Paramètres structuraux et/ou ultra-structuraux facteurs de la variabilité intra-arbre de l'anisotropie élastique du bois. Ann. For. Sci. 61:1–11.

Hölttä, T., T. Vesala, M. Perämäki and E. Nikinmaa. 2002. Relationships between embolism, stem water tension and diameter changes. J. Theor. Biol. 215:23–38.

Hunter, A.J. 2001. The distribution of mechanical stresses in the cell wall of wood induced by capillary tension in the lumen water—an approximate analysis. Wood Sci. Technol. 35:283–296.

Innes, T.C. 1995. Stress model of a wood fiber in relation to collapse. Wood Sci. Technol. 29:363–376.

Irvine, J. and J. Grace. 1997. Continuous measurements of water tension in xylem of trees based on the elastic properties of wood. Planta 202:455–461.

Klepper, B., D.V. Browning and H.M. Taylor. 1971. Stem diameter in relation to plant water status. Plant Physiol. 48:683–685.

Kozlowski, T.T. and C.H. Winget. 1964. Diurnal and seasonal variations in radii of tree stems. Ecology 45:149–155.

Neher, H.V. 1993. Effects of pressure inside Monterey pine trees. Trees 8:9–17.

Offenthaler, I., P. Hietz and H. Richter. 2001. Wood diameter indicates diurnal and long-term patterns of xylem water potential in Norway spruce. Trees 15:215–221.

Okuyama, T., M. Yoshida and H. Yamamoto. 1995. An estimation of turgor pressure change as one of the factors of growth stress generation in cell walls. Mokuzai Gakkaishi. 41:1070–1078.

Panterne, P., J. Burger and P. Cruiziat. 1998. A model of the variation of water potential and diameter within a woody axis cross-section under transpiration conditions. Trees 12:293–301.

Perämäki, M., E. Nikinmaa, S. Sevanto, H. Ilvesniemi, E. Siivola, P. Hari and T. Vesala. 2001. Tree stem diameter variations and transpiration in Scots pine: analysis using a dynamic sap flow model. Tree Physiol. 21:889–897.

Remorini, D. and R. Massai. 2003. Comparison of water status indicators for young peach trees. Irrig. Sci. 22:39–46.

Scholander, P.F., H.T. Hammel, E.A. Hemmingsen and E.D. Bradstreet. 1964. Hydrostatic pressure and osmotic potential in leaves of mangroves and some other plants. Proc. Nat. Acad. Sci. USA 52:119–125.

Sevanto, S., T. Vesala, M. Perämäki and E. Nikinmaa. 2002. Time lags for xylem and stem diameter variations in a Scots pine tree. Plant Cell Environ. 25:1071–1077.

Sevanto, S., T. Vesala, M. Perämäki and E. Nikinmaa. 2003. Sugar transport together with environmental conditions controls time lags between xylem and stem diameter changes. Plant Cell Environ. 26:1257–1265.

So, H.B., D.C. Reicosky and H.M. Taylor. 1979. Utility of stem diameter changes as predictors of plant canopy water potential. Agron. J. 71:707–713.

Tyree, M.T. and M.H. Zimmerman. 2002. Xylem structure and the ascent of sap. 2nd Edn. *In* Springer Series in Wood Science. Ed. T. Timell. Springer-Verlag, Berlin, 283 p.

Ueda, M. and E. Shibata. 2001. Diurnal changes in branch diameter as indicator of water status of Hinoki cypress *Chamaecyparis obtusa*. Trees 15:315–318.

Ueda, M. and E. Shibata. 2002. Water status of Hinoki cypress (*Chamaecyparis obtusa*) under reduced hydraulic conductance estimated from diurnal changes in trunk diameter. Trees 16:523–528.

Yamamoto, H. 1998. Generation mechanism of growth stresses in wood cell walls: roles of lignin deposition and cellulose microfibril during cell wall maturation. Wood Sci. Technol. 32:171–182.

Yamamoto, H., F. Sassus, M. Ninomiya and J. Gril. 2001. A model of anisotropic swelling and shrinking process of wood. Wood Sci. Technol. 35:167–181.

Yoshida, M., Y. Tamai, Y. Sano, M. Terazawa and T. Okuyama. 2000*a*. Seasonal change in tangential strain on the inner bark in white birch (*Betula platyphylla* var. *japonica*). Nagoya Univ. For. Sci. 19:21–28.

Yoshida, M., Y. Hosoo and T. Okuyama. 2000*b*. Periodicity as a factor in the generation of isotropic compressive growth stress between microfibrils in cell wall formation during a twenty-four hour period. Holzforschung 54:469–473.

Yoshida, M., O. Yamamoto and T. Okuyama. 2000*c*. Strain changes on the inner bark surface of an inclined coniferous sapling producing compression wood. Holzforschung 54:664–668.

## Appendix

*Kinematic compatibility inside a cylinder*

To ensure the continuity of the structure along direction *T*, any radial displacement $u_R(r)$ is associated to a tangential strain $\varepsilon_T(r)$, as demonstrated in Figure A1. Tangential strain can be computed as:

$$\varepsilon_T = \frac{(r+u_R)d\theta - r\,d\theta}{r\,d\theta}$$

This implies that:

$$\varepsilon_T(r) = \frac{u_R(r)}{r}$$

*Static equilibrium condition inside a cylinder*

The static equilibrium is ensured if the resultant of stresses acting at the boundaries of any elementary volume is null. As demonstrated in Figure A2, the resultant of the tangential component is ensured by symmetry, and that of the radial component is expressed as:

$$(r+dr)(\sigma_R + d\sigma_R)d\theta - r\sigma_R\,d\theta - \tfrac{1}{2}(2\sigma_T\,dr\,d\theta) = 0$$

This implies that:

$$\frac{d\sigma_R}{dr} + \frac{\sigma_R - \sigma_T}{r} = 0$$

*Constants of Equation 5*

$$\gamma^2 = \frac{C_{TT}}{C_{RR}}$$

$$K_\beta = \frac{\beta_T - \beta_R}{C_{RR}}$$

$$K_L = \frac{C_{TL} - C_{LR}}{C_{RR}}$$

*Coefficients of the displacement and stress fields*

$$a_i(r) = r^{\gamma_i} \qquad b_i(r) = r^{-\gamma_i}$$

$$c_i(r) = \frac{K_{L,i}}{1-\gamma_i^2} \qquad d_i(r) = \frac{r K_{\beta,i}}{1-\gamma_i^2}$$

$$e_i(r) = (\gamma_i C_{RR,i} + C_{RT,i})r^{\gamma_i - 1}$$

$$f_i(r) = (\gamma_i C_{RR,i} + C_{RT,i})r^{-\gamma_i - 1}$$

$$g_i(r) = C_{LR,i} + \frac{(C_{RR,i} + C_{RT,i})K_{L,i}}{1-\gamma_i^2}$$

$$h_i(r) = \beta_{R,i} + \frac{(C_{RR,i} + C_{RT,i})K_{\beta,i}}{1-\gamma_i^2}$$

$$j_i(r) = 2\pi\frac{\gamma_i C_{LR,i} + C_{TL,i}}{1+\gamma_i} r^{\gamma_i + 1}$$

$$k_i(r) = 2\pi\frac{-\gamma_i C_{LR,i} + C_{TL,i}}{1-\gamma_i} r^{-\gamma_i + 1}$$

$$l_i(r) = \pi\left(C_{LL,i} + \frac{C_{LR,i} + C_{TL,i}}{1-\gamma_i^2}K_{L,i}\right)r^2$$

$$m_i(r) = \pi\left(\beta_{L,i} + \frac{C_{LR,i} + C_{TL,i}}{1-\gamma_i^2}K_{\beta,i}\right)r^2$$

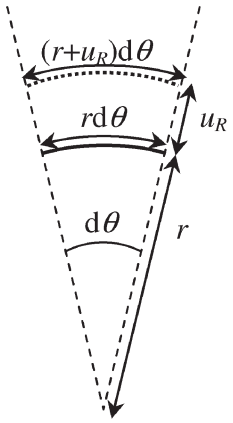


Figure A1. Relationship between tangential strain and radial displacement inside a cylinder.

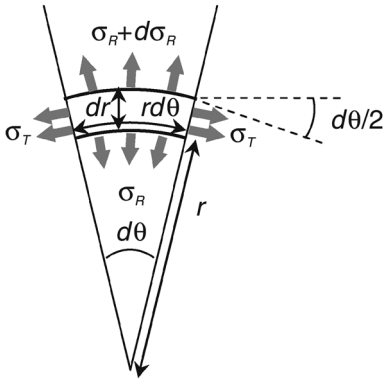


Figure A2. Static equilibrium of an elementary volume of the cylinder.

Table A1. List of symbols.

| Symbol | Description |
|---|---|
| $R, T, L$ | Radial, tangential and longitudinal directions |
| $r, t, l$ | Radial, tangential and longitudinal positions |
| $(u_R, u_T, u_L)$ | Displacement vector |
| $(\varepsilon_R, \varepsilon_T, \varepsilon_L)$ | Strain vector |
| $(\sigma_R, \sigma_T, \sigma_L)$ | Stress vector (elastic stress) |
| $(\beta_R, \beta_T, \beta_L)$ | Induced stress vector (inelastic stress) |
| $C_{XY,i}$ | Stiffness term $X, Y = (R, T, L)^2$ of the $i$th layer |
| $r_i$ | External radius of the $i$th layer |
| $\gamma_i$ | Anisotropy coefficient of the $i$th layer ($\gamma_i = \sqrt{C_{TT,i}/C_{RR,i}}$) |
| $K_{\beta,i}, K_{L,i}$ | Constants depending on stiffness and induced stress of the $i$th layer |
| $A_i, B_i$ | Integrations constants of the $i$th layer |
| $u_o, u_n$ | Conditions in radial displacement at the internal and external radial bound |
| $\sigma_o, \sigma_n$ | Conditions in radial stress at the internal and external radial bound |
| $N$ | Longitudinal condition of axial load |
| $a_i, b_i, c_i, d_i$ | Coefficients of the expression of radial displacement |
| $e_i, f_i, g_i, h_i$ | Coefficients of the expression of radial stress |
| $j_i, k_i, l_i, m_i$ | Coefficients of the expression of longitudinal stress |
| $P$ | Change in hydrostatic pressure |
| $\pi$ | Change in osmotic potential |
| $d$ | Basic density of the plant material |
| $d_o$ | Basic density of the cell wall material |
| $\rho$ | Radius ratio of the cell ($\rho = r_o/r_n$) |
| $k$ | Transverse stress transmission factor |
| $k_R, k_T, k_L$ | Anisotropic stress transmission factors (in the macroscopic reference system) |